Earth and Space Science

RESEARCH ARTICLE
10.1029/2024EA003577

A Bayesian Model for 20th Century Antarctic Sea Ice Extent Reconstruction

T. J. Maierhofer[1], M. N. Raphael[2], R. L. Fogt[3], and M. S. Handcock[1]

[1]Department of Statistics, University of California Los Angeles, Los Angeles, CA, USA, [2]Department of Geography, University of California Los Angeles, Los Angeles, CA, USA, [3]Department of Geography and Scalia Laboratory for Atmospheric Analysis, Ohio University, Athens, OH, USA

Key Points:

- Introduction of statistical model for ensemble reconstruction of Antarctic sea ice extent
- Reconstruction of unobserved 20th century Antarctic sea ice extent and imputation of missing values in satellite observed period
- Bayesian framework creates plausible reconstructions of Antarctic sea ice by sector displaying realistic spatio-temporal autocorrelation

Supporting Information:

Supporting Information may be found in the online version of this article.

Correspondence to:

T. J. Maierhofer,
thomas.maierhofer@stat.ucla.edu

Citation:

Maierhofer, T. J., Raphael, M. N., Fogt, R. L., & Handcock, M. S. (2024). A Bayesian model for 20th century Antarctic sea ice extent reconstruction. *Earth and Space Science*, *11*, e2024EA003577. https://doi.org/10.1029/2024EA003577

Received 23 FEB 2024
Accepted 19 SEP 2024

Author Contributions:

Conceptualization: T. J. Maierhofer, M. N. Raphael, M. S. Handcock
Data curation: T. J. Maierhofer, R. L. Fogt, M. S. Handcock
Formal analysis: T. J. Maierhofer, R. L. Fogt, M. S. Handcock
Funding acquisition: M. N. Raphael, R. L. Fogt, M. S. Handcock
Investigation: T. J. Maierhofer, M. N. Raphael, R. L. Fogt, M. S. Handcock
Methodology: T. J. Maierhofer, M. N. Raphael, R. L. Fogt, M. S. Handcock
Project administration: M. N. Raphael, R. L. Fogt, M. S. Handcock
Resources: T. J. Maierhofer, M. N. Raphael, R. L. Fogt, M. S. Handcock

Abstract

Antarctic sea ice, a key component in the complex Antarctic climate system, is an important driver and indicator of the global climate. In the relatively short satellite-observed period from 1979 to 2022 the sea ice extent has continuously increased (contrasting a major decrease in Arctic sea ice) up to a dramatic decrease between 2014 and 2017. Recent years have seen record sea ice lows in February 2022–February 2023. We use a statistical ensemble reconstruction of Antarctic sea ice to put the observed changes into the historical context of the entire 20th century. We propose a seasonal Vector Auto-Regressive Moving Average (VARMA) model fit in a Bayesian framework using regularized horseshoe priors on the regression coefficients to create a stochastic ensemble reconstruction of monthly Antarctic Sea ice extent from 1900 to 1979. This novel model produces a set of 2,500 plausible sea ice extent reconstructions for the sea ice by sector that incorporate the autocorrelation structure of sea ice over time as well as the dependence of sea ice between the sectors. These fully observed reconstructions exhibit plausible month-to-month changes in reconstructed sea ice as well as plausible interactions between the sectors and the total. We reconstruct an overall higher sea ice extent earlier in the 20th century with a relatively sharp decline in the 1970s. These trends agree well with previous reconstructions of Antarctic sea ice based on ice core data, whaling locations, and climatological data, as well as early satellite observations in the reconstruction period.

Plain Language Summary

Antarctic sea ice, a key component in the complex Antarctic climate system, is an important driver and indicator of the global climate. In the relatively short satellite-observed period from 1979 to 2022 the sea ice extent has continuously increased (contrasting a major decrease in Arctic sea ice) up to a dramatic decrease between 2014 and 2017. Recent years have seen record sea ice lows in February 2022 and February 2023. We reconstruct the Antarctic sea ice extent to put the observed changes into the historical context of the entire 20th century. We propose a novel statistical model to create multiple reconstructions of monthly Antarctic Sea ice extent from 1900 to 1979. This state-of-the-art model produces a set of 2,500 plausible sea ice extent reconstructions that exhibit plausible month-to-month changes in reconstructed sea ice as well as plausible interactions between the sectors and the total. We reconstruct an overall higher sea ice extent earlier in the 20th century with a relatively sharp decline in the 1970s. These trends agree well with previous reconstructions of Antarctic sea ice based on ice core data, whaling locations, and climatological data, as well as early satellite observations in the reconstruction period.

1. Introduction

Antarctic sea ice is a key component of the Southern Hemisphere climate system, but has largely been unobserved before the start of the modern satellite record with the launch of NIMBUS-7 in October 1978. Estimation of the sea ice concentration on a continental scale in Antarctica is only feasible using remote sensing (i.e., satellites) due to its vastness and remoteness. Since 1978, images that can be used to estimate the Antarctic sea ice concentration are available on a 1 to 2 day resolution (Meier et al., 2016). Detailed analysis of Antarctic sea ice variability over the satellite-observed period shows that it is mainly driven by its strong annual cycle. Total Antarctic sea ice extent ranges from about 3 million km^2 in February to about 19 million km^2 in September, a difference of about twice the land area of the contiguous United States. After accounting for this strong annual cycle, a small long term positive linear trend has been identified in the Antarctic sea ice extent from 1980 to 2014, contrasting with a decline in Arctic sea ice of much larger magnitude. This positive trend is subject to strong regional trends of opposing nature, in particular a sea ice decrease in the Amundsen-Bellingshausen Sea, emphasizing the importance of analyzing the Antarctic sea ice extent by sector. To understand the full merit of our approach it is helpful

Software: T. J. Maierhofer, R. L. Fogt, M. S. Handcock
Supervision: M. N. Raphael, M. S. Handcock
Validation: T. J. Maierhofer, R. L. Fogt, M. S. Handcock
Visualization: T. J. Maierhofer, M. S. Handcock
Writing – original draft: T. J. Maierhofer, M. N. Raphael, M. S. Handcock
Writing – review & editing: T. J. Maierhofer, M. N. Raphael, R. L. Fogt, M. S. Handcock

to place the task of Antarctic sea ice reconstruction into the field of statistics. Antarctic sea ice extent is a time series, a multivariate time series if analyzed by sector as is the case paper. This is relevant, as multivariate time series modeling allows the estimation and incorporation of temporal and spatial autocorrelation, here sea ice extent of neighboring months and different sectors are correlated. The task of reconstruction can be viewed as a missing data problem, specifically an imputation, see Rubin and Little (2019) for a comprehensive review of the field of missing data. It makes sense to treat reconstruction as a missing data problem as opposed to a time series prediction or forecasting problem, as we have observations of our predictor variables throughout the reconstruction period. Additionally, there are a few missing months during the satellite-observed period as well that need to be imputed. The Antarctic sea ice extent is missing at random (MAR) with the missingness exclusively depending on time (missing before the start of the satellite record, observed afterward), but not on any other observed or unobserved variables or the sea ice itself, which provides the theoretical basis for asymptotically unbiased estimation. There are many strategies to imputing missing values, with using regression predictions to perform deterministic imputation being the current state-of-the-art in the Antarctic sea ice literature. This approach underestimates the variability in reconstructions, as the predicted values from the regression tend to be much less variable than the original data. As a showcase, consider a regression model with an R^2 of 30%, a good coefficient of determination in the context of Antarctic sea ice reconstruction. This value means that this model explains 30% of the variance in Antarctic sea ice (or 54% of its standard deviation), which means that its predictions will have a variance of only about 30% of the original variance. Using this model's predictions will severely underestimate the variability in reconstructed sea ice and have a strong tendency to predict values close to the climatology. This modeling approach is used in most papers in the literature. A next step would be so called random regression imputation, where the unexplained variability is added on top of the regression prediction's deterministic imputations. Ideally, this step is repeated multiple times, resulting in multiple imputations with different random errors added to the deterministic predictions. In particular in the context of time series reconstructions, we can do better, as the error terms in our regression model are not independent between temporally and spatially close observations. Our choice of fitting a regression model in a Bayesian framework naturally creates multiple imputations of missing values (all values in the reconstruction period as well as the missing values in the satellite observed period) by explicitly modeling reconstruction uncertainty in average reconstructions as well as spatio-temporally autocorrelated random errors.

Pre-satellite-era Antarctic sea ice has previously been reconstructed in a number of papers (Abram et al., 2010, 2011; Becagli et al., 2009; Cotté & Guinet, 2007; Curran et al., 2003; Dalaiden et al., 2021; De la Mare, 1997, 2009; Fogt et al., 2022; W. Hobbs et al., 2016; Meyerson et al., 2002; Porter et al., 2016; Sinclair et al., 2014; Thomas & Abram, 2016; Thomas et al., 2019; Yang et al., 2021), but we present the first monthly ensemble reconstruction for Antarctic sea ice extent by sector and in total for the entire 20th century. Previous reconstructions generally agree that Antarctic sea ice extent was higher in the first half of the 20th century than in the second half, but different reconstructions vary on the exact scale of this sea ice decline. This general decline is captured in our reconstructions as well as local trends on a smaller time-scale. De la Mare (1997), Cotté and Guinet (2007) and De La Mare (2009) model discrete sections of 10° longitude and 10 day periods without taking into account the considerable spatio-temporal correlations of nearby longitudes and days of year. Our model improves upon this by explicitly modeling the covariance between sectors as well as the temporal autocorrelation structure of Antarctic sea ice. This allows us to create an ensemble of realistic reconstructions of Antarctic sea ice, as opposed to an average reconstruction with an uncertainty estimate. Local sea ice reconstructions have been created using a series of ice cores Meyerson et al. (2002), Curran et al. (2003), Becagli et al. (2009), Abram et al. (2010, 2011), Sinclair et al. (2014), Porter et al. (2016), W. Hobbs et al. (2016) and Thomas and Abram (2016). However, it is complicated to reconstruct sectoral and total Antarctic sea ice extent from the available set of ice core data as the uncertainty of the reconstructions is large (Maierhofer, 2023, Chapter 3.2). Another drawback is that only an average sea ice extent has been reconstructed and major improvements need to be made regarding uncertainty estimation, external and internal validation, and the temporal autocorrelation structure of Antarctic sea ice. For a review of this research, see Abram et al. (2013) and Thomas et al. (2019).

Dalaiden et al. (2021) reconstruct regional Antarctic sea ice on an annual resolution based on ice cores and tree ring widths using a Bayesian framework. They use the Bayesian framework to incorporate multiple simulated runs from a climate simulation model (isotope-enabled Community Earth System Model version 1, iCESM1; Brady et al., 2019) as a prior distribution for Antarctic sea ice during the reconstruction period. Using a climate model trained on satellite observations to create a prior distribution means that information from the data (the

observed satellite record) is used to create the prior distribution, which is less than ideal as the prior distribution should represent the state of knowledge before observing the data. Their approach preserves spatial autocorrelation in sea ice, but neglects temporal autocorrelation. This means that their individual reconstructions are not reported, but only the reconstruction average with uncertainty bands.

Fogt et al. (2022) reconstruct Antarctic sea ice by sector and season for the 20th century using temperature and sea level pressure (SLP) recorded by weather stations in the Southern Hemisphere as compiled in Fogt et al. (2016). Each season and sector are modeled and reconstructed completely independently, ignoring their spatio-temporal correlation. Fogt et al. (2022) provide ensemble reconstructions by replicating their reconstruction model for different subsets of covariates, but implicit biases in the selection of covariates lead to an underestimation of reconstruction uncertainty. Their approach incorporates some reconstruction uncertainty in average reconstructions but neglects the reconstruction uncertainty in the unexplained error terms. The completely separate reconstruction for each season is useful for seasonal analyses but leads to disjoint reconstructions between neighboring seasons (i.e., Spring and Summer of 1962 are modeled and reconstructed completely separately) with no matching or continuity between reconstructions.

A particular strength of our reconstruction is its implementation in a Bayesian statistical framework, see Gelman et al. (2004) for an introduction, allowing us the sampling of arbitrary numbers of complete time series of plausible reconstructions of Antarctic sea ice, its overall evolution, and in particular its month-to-month progression in each reconstruction. The more commonly used Frequentist framework creates an average reconstruction and estimates its uncertainty, without creating time series of complete reconstructions. This is certainly useful for describing average trends, but cannot answer research questions pertaining to individual reconstructions and their variability. The possibility to compare observed events to individual reconstructions is lost. Our reconstructions incorporate the entire information provided by weather stations in the Southern Hemisphere compiled by Fogt et al. (2016), show realistic spatial correlation patterns between sectors as well as realistic temporal autocorrelation patterns for neighboring months within sectors, while faithfully including reconstruction uncertainty. A set of these reconstructions as well as the reconstruction mean are shown in Figures 4 and 5. Our ensemble of 2,500 reconstructions for each sector and in total are publicly available (Maierhofer, 2023).

2. Modeling Framework

As an overall modeling framework we consider multivariate dynamic spatio-temporal (MDST) models. MDST models enables us to jointly represent the observed data variables and flexibly connect them to the underlying climate processes. We can then better model the underlying climate process and produce better reconstructions than a model for the observed data variables alone. The relationship among the observed data variables is clouded by their measurement and other errors. Let Z_t be the multivariate observation vector at time (i.e., month) $t = 1,\ldots, T$, where $t = 1$ corresponds to January 1900, and T corresponds to the most recent observation month we have. In our model, Z_t will include the observed sea ice extent, observed sea ice concentrations, SLP, etc, or transformations of them. Our primary interest is in a latent multivariate spatio-temporal process, Y_t, representing the spatio-temporal state of the climate system. We consider models relating the observed data to the underlying state of the climate system (so called, state-space models):

$$Z_t = H(Y_t; \theta_H; \epsilon_t) \qquad t = 1, \ldots, T, \tag{1}$$

and a model for the evolution of the climate system:

$$Y_t = M\big(Y_{t-1}; \theta_M; \eta_t\big), \tag{2}$$

where Y_t is the state vector, $H(\cdot)$ is the observation function with parameters θ_H and error process ϵ_t, and $M(\cdot)$ is the state transition function depending on parameters θ_M and noise process η_t (West & Harrison, 2006). An essential further assumption of the model is that the observation vectors at different times are conditionally independent given the state-process and that the state-process follows a first-order Markov assumption (i.e., the dependence of the state process on its past is captured by the previous month). We relax the first-order Markov assumption as the data suggest it. In general, the MDST can capture linear, non-linear, deterministic or stochastic

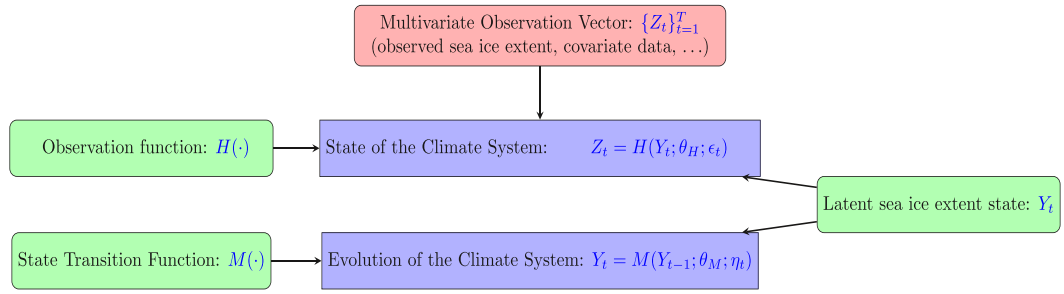

Figure 1. Graphical representation of the model expressed by Equations 1 and 2. The observed sea ice extent for the five sectors along with the station and index covariate data is represented by Z_t at each time point $t = 1, \ldots, T$. The primary variable of interest is the (latent) sea ice extent within each sector at time t, represented by Y_t. These are linked by the models for the state of the climate system and its dynamics/evolution. These, in turn, are specified by the observation function, the state transition function and related parameters.

relationship through the choice of the functions $H(\cdot)$ and $M(\cdot)$. This observation function relates the state process to the data and can represent transformation, dimension reduction, etc, as the process evolves over time. The state transition function evolves the process forward in time, capturing the multivariate dynamics and dependencies. It is important to note that, under these assumptions, the state-space model enables us to specify the full joint distribution of the observed data and state process, that is, $Z_1, Z_2, \ldots, Z_T, Y_1, Y_2, \ldots, Y_T$. Thus, we have a stochastic model of spatio-temporal variation of the variables we wish to reconstruct (e.g., sea ice) and the variables we wish to use for that reconstruction (e.g., SLP, temperature, climate indices).

We first consider multivariate linear models for the relationship between the observed data and the state of the climate system:

$$Z_t = X_t\beta + H_t(\theta_h)\, Y_t + \epsilon_t \qquad t = 1, \ldots, T \tag{3}$$

where X_t is a vector of known (external or exogenous) covariates and β are the regression coefficients. These exogenous covariates represent large-scale spatio-temporal features such as seasonality, time trends, or even the shape of the Antarctic continent, etc. Here $H_t(\theta_h)$ is a (observation) process matrix. The error process ϵ_t is typically independent of Y_t, independent in time and has zero mean. We can also consider multivariate linear models for the evolution of the climate state process:

$$Y_t = M_t(\theta_M)\, Y_{t-1} + \eta_t \qquad t = 1, \ldots, T, \tag{4}$$

where $M_t(\theta_M)$ is the climate process matrix and η_t is a noise process that is typically independent of Y_{t-1}, independent in time and has zero mean. Many simple choices of $M_t(\theta_M)$ have been considered (Huang & Cressie, 1996).

The model expressed by Equations 1 and 2 is graphically represented in Figure 1. This model has a number of important connections and advantages relative to existing approaches for reconstruction:

1. The observation equation, for example, Equation 1, naturally represents the measurement error in the data. Previous methods have attempted to adjust for measurement error in the "independent" variables using geometric mean regression (Abram et al., 2010; Thomas & Abram, 2016). Our approach is more flexible and allows for complex and dependent measurement errors for the variables.
2. The observation equation allows the relationship between the sea ice and the predictor variables to be expressed through their less variable state process versions (e.g., a state variable close to the yearly average of ice core MSA) rather than just the noisy observed value.
3. The model can be thought of a more sophisticated stochastic process version of the canonical correlation analysis currently used in sea ice reconstruction (Krawczyk et al., 2017).
4. The state process model, for example, Equation 2, represents the influence of time lagged effects where the lags can be month-to-month and cross-variable lags (e.g., sea surface temperature in the prior month on sea ice extent this month).

5. The model naturally accommodates missing data on the variables (e.g., sea ice extent in parts of 1987 or sea surface temperature). These will be treated as unknown quantities when the model parameters are estimated.

We now reduce this general model to the problem of predicting Antarctic sea ice extent in five sectors using temperature and SLP measurements from weather stations in the Southern Hemisphere. Let $Y_t(s)$ be the value of a spatio-temporal process at location $s \in \{s_1, \ldots, s_{N_Y}\}$ so that $Y_t = \{Y_t(s)\}_{s=1}^{s_{N_Y}}$. Let $X_t(s)$ be the N_X dimensional observation of a spatio-temporal covariate process so that $X_t = \{X_t(s)\}_{s=1}^{s_{N_X}}$ Specifically, let $Y_t(s)$ be the monthly sea ice extent at time $t \in$ {January 1900, February 1900, …, December 2020} for sector $s \in$ (King Haakon VII, Ross-Amundsen Sea, East Antarctica, Weddell Sea, Amundsen-Bellingshausen Sea). The sea ice is thus a 5 dimensional spatial time series and we adopt the notation $Y_{s,t}$ for sector s at time t or Y_t for short.

We fit our model on monthly standardized anomalies due to the strong annual cycle in Antarctic sea ice. For each month across all years we compute the average sea ice extent and its standard deviation, which we use to standardize the observations in our data set for the purpose of modeling. For the purposes of reporting results and evaluating prediction accuracy we re-transform our reconstructions to sea ice extent anomaly in million km^2 by multiplying the model predictions with the monthly standard deviations. Out model is seasonally varying, but does not allow coefficients to change over time. This implies the common assumption that the relationship between the atmosphere as measured by temperature and SLP and the Antarctic sea ice extent is stable over time.

Fitting our model in a Bayesian framework is an elegant choice for our application. For estimating the model parameters, it naturally allows us to incorporate prior knowledge of model parameters in the form of prior distributions. Most prominently, we know that the sea ice only has a weak relationship with measurements from each individual station in the Southern hemisphere and that the sea ice in many sectors is totally unrelated to weather measured by geographically distant stations in other sectors. Additionally, a Bayesian framework naturally incorporates model uncertainty, parameter uncertainty, and unexplained variability in its predictions, in our case the reconstructed sea ice. A last but maybe most important argument for the Bayesian framework is that it automatically provides an ensemble of reconstructions, that is, many plausible reconstructions for all sectors over the entire time period. These ensembles incorporate all sources of uncertainty and can readily be used in further analyses. Each individual reconstruction has a plausible month-to-month progression and overall trend for the sea ice in each sector and incorporates credible relationships between the reconstructions in each sector.

The model we propose for Antarctic sea ice reconstruction is a seasonal VARMA (vector auto-regressive moving average) model fit in a Bayesian framework using regularized horseshoe priors on the regression coefficients. The model needs to be a Vector ARMA model due to the target variable, the sea ice in all five sectors, being a multivariate vector. Modeling the five sectors independently would neglect the correlation between them, leading to implausible joint behavior of the reconstructions and inaccurate variability in the reconstructed total sea ice extent as the sum of all sectors. We chose a Vector **Auto-Regressive Moving-Average** model because the target variable is a time series. Time series in general, and sea ice extent is no exception, tend to be autocorrelated, meaning consecutive measurements in the time series are correlated with each other, and consecutive residuals in time series models are correlated as well. Explicitly modeling this self-dependency will result in reconstructions with plausible month-to-month progressions and plausible deviations from overall trends. Putting a regularized horseshoe prior (Piironen & Vehtari, 2017) on regression coefficients is a state-of-the-art method to ensure identifiability and sparsity in Bayesian regression models. The regularized horseshoe prior shrinks most coefficients either to zero (no effect) or leaves them almost unpenalized (almost full effect). This is plausible in this scenario where we expect measurements of most weather stations to have no association whatsoever with the sea ice extent in a specific sector, but some stations might have reasonably strong predictive power.

Before introducing our model in Section 2.5, we first review its individual modeling components, the multivariate regression model (Section 2.1), the VARMA model (Section 2.2), the seasonal regression model (Section 2.3), and the regularized horseshoe prior (Section 2.4).

2.1. Multivariate Regression Model

Recall the multivariate regression model

$$Y_t = HX_t + \varepsilon_t \tag{5}$$

at time t with multivariate target variable $Y_t \in \mathbb{R}^{N_Y \times 1}$, multivariate predictor variables $X_t \in \mathbb{R}^{N_X \times 1}$, coefficient matrix $H \in \mathbb{R}^{N_Y \times N_X}$ and error term $\varepsilon_t \in \mathbb{R}^{N_Y \times 1}$ which follow a multivariate Gaussian distribution centered around zero

$$\varepsilon_t \sim N_{N_Y}(0, \Sigma), \forall t \tag{6}$$

with positive semidefinite covariance matrix $\Sigma \in \mathbb{R}^{N_Y \times N_Y}$.

2.2. Vector Autoregressive Moving Average Model

Building upon the multivariate regression model, recall the VARMA(p, q) model with p autoregressive terms and q moving-average terms of the form

$$Y_t = c + \sum_{i=1}^{p} A_{i,\cdot}\, Y_{t-i} + \sum_{j=1}^{q} B_{j,\cdot}\varepsilon_{t-j} + \varepsilon_t, \tag{7}$$

with $A_{i,}$ denoting the ith row of the autoregressive coefficient matrix $A \in \mathbb{R}^{p \times N_Y}$ and $B_{j,}$ denoting the jth row of the moving average coefficient matrix $B \in \mathbb{R}^{q \times N_y}$.

2.3. Seasonally Varying Model

Recall the univariate seasonally varying regression model for monthly data

$$Y_t = f(\text{month}(t))\, X_t + \varepsilon_t, \tag{8}$$

where $f : [1, 12] \to \mathbb{R}$ is a smooth cyclical function describing the regression coefficient of $X_t \in \mathbb{R}$ on $Y_t \in \mathbb{R}$ for every month of year month(t) $\in [1, 12]$. The coefficient function f has to be smooth because the effect of covariates should be similar in neighboring months and cyclical because December (month 12) and January (month 1) are neighboring.

Due to the strong seasonality of the Antarctic climate system we extend the VARMA(p, q) model to allow seasonally varying autoregressive and moving-average terms. For every month $k = \text{month}(t) \in [1, 12]$ and lag $l = 1, \ldots, p$, and sector s we estimate the autoregressive coefficient $A_{l,s,k}$. Using the same generalization on the moving average coefficients, we formulate a seasonally varying VARMA model as

$$Y_t = c + \sum_{i=1}^{p} A_{i,\cdot\,\text{month}(t)}\, Y_{t-i} + \sum_{j=1}^{q} B_{j,\cdot\,\text{month}(t)}\varepsilon_{t-j} + \varepsilon_t. \tag{9}$$

2.4. Regularized Horseshoe Prior

The regularized horseshoe prior Piironen and Vehtari (2017) is a useful tool to enforce sparsity in the coefficients β of a regression model of the form

$$Y_t = \beta X_t + \varepsilon_t,\ t = 1, \ldots, T \tag{10}$$

where $Y_t \in \mathbb{R}$, $\beta \in \mathbb{R}^{N_X}$, $X_t \in \mathbb{R}^{N_X}$, and $\varepsilon_t \in \mathbb{R}$. Model sparsity is particularly important when we have fewer observations than covariates $T < N_X$, or when many covariates can be assumed to have no impact $(\beta_m = 0)$ on the target variable. Both of these conditions are met in our case. The regularized horseshoe is an extension of the horseshoe prior (Carvalho et al., 2010) that puts a prior on the regression coefficients $\beta_m, m = 1, \ldots, N_X$, shrinking all β toward zero and setting some of them to be exactly equal to zero. The unregularized horseshoe is of the form.

$$\beta_m \sim N\left(0, \tau^2\lambda_m^2\right) \tag{11}$$

$$\lambda_m \sim \text{Half-Cauchy}(0, 1) = \text{Half-Student } t_1(0, 1) \tag{12}$$

With local horseshoe parameter λ_m controlling the local shrinkage and global horseshoe parameter τ controlling the overall shrinkage. While the global horseshoe parameter τ pulls all coefficients toward zero for small values of τ, the thick Cauchy-tails of the local horseshoe parameters λ_m allow some coefficients β_m to be almost unaffected. The regularized horseshoe is an extension of the horseshoe prior containing an additional regularization parameter c controlling the shrinkage of large parameters that would be unaffected by the unregularized horseshoe prior. It is of the form.

$$\beta_m \sim N\left(0, \tau^2 \tilde{\lambda}_m^2\right) \tag{13}$$

$$\tilde{\lambda}_m^2 = \frac{c^2 \lambda_m^2}{c^2 + \tau^2 \lambda_m^2} \tag{14}$$

$$\lambda_m \sim \text{Half-Cauchy}(0, 1) = \text{Half-Student } t_1(0, 1) \tag{15}$$

With regularized horseshoe parameter $\tilde{\lambda}_m$ controlling the shrinkage via the local horseshoe parameter λ_m controlling the local shrinkage, global horseshoe parameter τ controlling the overall shrinkage, and regularization parameter c controlling the shrinkage for $\lambda_m \to 0$ when the unregularized horseshoe would not shrink the parameter at all. For small coefficients β_m with strong shrinkage $\tau^2 \lambda_m^2 \ll c^2$, the regularized horseshoe parameter converges to the unregularized horseshoe parameter $\tilde{\lambda}_m \to \lambda_m$. For large coefficients β_m with weak shrinkage $\tau^2 \lambda_m^2 \gg c^2$, the regularized horseshoe parameter $\tilde{\lambda}_m^2 \to c^2/\tau^2$ and the resulting prior distribution converges to

$$\beta_m \sim N(0, c^2), \tag{16}$$

making c^2 the shrinkage parameter of an otherwise unregularized coefficient. Our implementation follows the alternative parametrization proposed in Peltola et al. (2014) and code is provided upon request. A Half-Cauchy prior is put on the global shrinkage parameter τ

$$\tau \sim \text{Half-Cauchy}(0, \tau_0), \tag{17}$$

where the scale parameter τ_0 determines the overall shrinkage, that is, what proportion of coefficients β will be set to zero. The regularization parameter c^2 is chosen according to an inverse gamma distribution

$$c^2 \sim \text{Inverse Gamma}(0.5\nu, 0.5\nu). \tag{18}$$

which translates to a Student $t_\nu(0,1)$ distribution with ν° of freedom for coefficients β_m far from zero, because the inverse gamma distribution as a prior on an unknown variance (Equation 18) in a Gaussian distribution (Equation 16) results in a Student's t posterior distribution.

2.5. Complete Model

In this section we assemble our full model, a seasonal VARMA model in a Bayesian framework using regularized horseshoe priors on the regression coefficients, from its parts presented in the previous Sections 2.1–2.4. For sea ice $Y_{s,t}$ in sector s at time t our model takes the form

$$Y_{s,t} = \sum_{k=1}^{N_X} f_k(\text{month}(t)) X_{k,t} + \sum_{i=1}^{p} A_{i,s,\text{month}(t)}\, Y_{s,t-i} + \sum_{j=1}^{q} B_{j,s,\text{month}(t)} \varepsilon_{s,t-j} + \varepsilon_{s,t}, \tag{19}$$

where the error terms ε_t at time t follow a multivariate Gaussian distribution centered around zero

$$\varepsilon_t \sim N_{N_Y}(0, \Sigma), \ \forall\, t \tag{20}$$

with positive semidefinite covariance matrix $\Sigma \in \mathbb{R}^{N_Y \times N_Y}$.

The seasonally varying regression coefficients f_k are implemented as cyclical splines with four basis functions. A horseshoe prior is set on these splines coefficients that creates sparsity in the coefficients. The model used to create the reconstructions reported here does not have seasonally varying regression coefficients. Even though there is strong evidence for the relationship between atmosphere and Antarctic sea ice being seasonal (e.g., W. R. Hobbs et al., 2015), we find that seasonally varying regression coefficients are not warranted with the short observed record and the huge number of predictor variables to choose from. After accounting for seasonal variability through monthly standardization of the Antarctic sea ice extent, we found only insubstantial changes in our results when using seasonally varying regression varying coefficients at a dramatic computational burden.

Even though seasonally varying regression coefficients are not warranted in this application, we find that seasonally varying autoregressive coefficients are required. To ease the burden of computation we use strong priors to shrink the seasonally varying autoregressive terms toward their overall mean per lag and season $\tilde{A}_{l,s}$. For each lag l we specify a multivariate Gaussian prior for the mean autoregressive coefficient across all sectors,

$$\tilde{A}_{l,\cdot} \sim N_{N_Y}\left(0, \begin{bmatrix} v_s & & 0 \\ & \dots & \\ 0 & & v_s \end{bmatrix}\right), \tag{21}$$

with prior variance parameter v_s regulating the shrinkage. This specification allows us to borrow power across sectors, which is useful, as the autoregressive coefficients for each lag tend to be similar in all sectors. For the seasonally varying autoregressive terms we specify a multivariate Gaussian prior of the form

$$A_{l,s,\cdot} \sim N_{12}\left(\tilde{A}_{l,s}, \begin{bmatrix} v & c & 0 & \dots & 0 & c \\ c & v & c & 0 & \dots & 0 \\ 0 & c & v & c & 0 & \dots \\ \dots & 0 & c & v & \dots & 0 \\ 0 & \dots & \dots & \dots & \dots & c \\ c & 0 & \dots & 0 & c & v \end{bmatrix}\right). \tag{22}$$

This prior specification implies shrinkage of the seasonal coefficients toward their overall mean $\tilde{A}_{l,s}$. The covariance matrix has the shrinkage parameter v on the diagonal regulating how much the seasonal coefficients can vary from their overall mean. On the off-diagonal and in the bottom left and top-right corner is the covariance parameter c which is used to enforce smoothness across neighboring months. Note that the first month January and the last month December are neighboring.

The final model has a huge number of parameters but the strong priors imposed on them result in stable parameter estimates and reconstructions. All model parameters are sampled using the Hamiltonian Monte Carlo algorithm implemented in the software package Stan (Stan Development Team, 2022). We draw 2,500 sets of parameters giving a good estimate of their joint posterior distribution. These 2,500 parameter sets correspond to 2,500 models and 2,500 reconstructions, which are interpreted in Section 4.

3. Data

Our sea ice reconstructions involves a large set of climatological data across the Southern Hemisphere. We use monthly sea-level-pressure and temperature records from weather stations in the Southern hemisphere to train our model to predict satellite-observed Antarctic sea ice extent from 1979 to 2020. The longer historical record of weather stations informs our model's sea ice reconstructions for the entire 20th century.

3.1. Antarctic Sea Ice

The satellite observed sea ice data form the core of our reconstruction procedure, as they are the calibration data set used for modeling the relationship between sea ice and the climatological data in the satellite era. The monthly sea

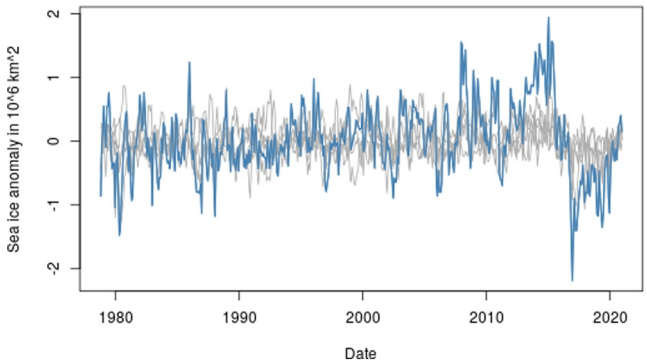

Figure 2. Sea ice extent anomaly in million km^2 by sector (gray) and in total (blue) over the course of the observation period 1979–2020. Note the larger magnitude of total sea ice variability due to positively correlated sectoral sea ice anomalies.

ice extent is computed from the Nimbus-7 Scanning Multichannel Microwave Radiometer and the Defense Meteorological Satellite Program Special Sensor Microwave Imager-Special Sensor Microwave Imager/Sounder (SSM/I-SSMIS). We used the climate data record (CDR) daily concentration fields from the NOAA/NSIDC CDR of Passive Microwave Sea Ice Concentration, Version 4 (https://nsidc.org/data/g02202; Meier et al., 2016). This data set provides sea ice concentrations on the SSM/I-SSMIS polar stereographic grid (25 km × 25 km) from 25 October 1978 to 31 December 2020 and are daily except before July 1987, when they are given every other day. We use the 15% sea ice concentration isoline as the sea ice edge and compute the sea ice extent as the sum of the area of each grid cell to its South, which may include polynyas and other enclosed areas of lower sea ice concentration. There is a gap in the observations from 3 December 1987 to 12 January 1988 and every other day is missing from 1978 to 1987. For these missing days the sea ice extent is stochastically imputed using a daily version of the monthly Bayesian Auto-Regressive Integrated Moving Average (ARIMA) model used for the reconstruction itself (Detailed in Section 2). This retains more information than treating the corresponding months as missing and there is negligible variation in monthly reconstructions across multiple daily imputations of these missing values. Based on the completed daily sea ice extent record, we compute monthly sea ice extent as the average of all days within each month. Sea ice anomalies are computed by subtracting an invariant annual cycle computed analogously to Handcock and Raphael (2020). The sea ice extent by sector is computed as the sum of the area of each grid cell South of the sea ice edge within each sector, using the sea ice based sectors introduced in Raphael and Hobbs (2014). They defined these sectors based upon the coherent variability within the sea ice. These sectors shown in Figure 3 are identified by their longitudinal range as follows: Ross-Amundsen Sea (162°E−250°E), Amundsen–Bellingshausen Sea (250°E−290°E), Weddell Sea (290°E−346°E), King Haakon VII (346°E−71°E), and East Antarctica (71°E−162°E). Note that this definition ensures the total sea ice extent is exactly equal to the sum of the sea ice extent in all five sectors.

The sea ice extent anomalies by sector and in total are depicted in Figure 2. The magnitude of the extrema in total sea ice anomaly (blue) tend to be larger than in any individual sector (gray). The covariance matrix for the sea ice extent anomalies in million km^2 are reported in the top half of Table 1. We report a covariance matrix as opposed

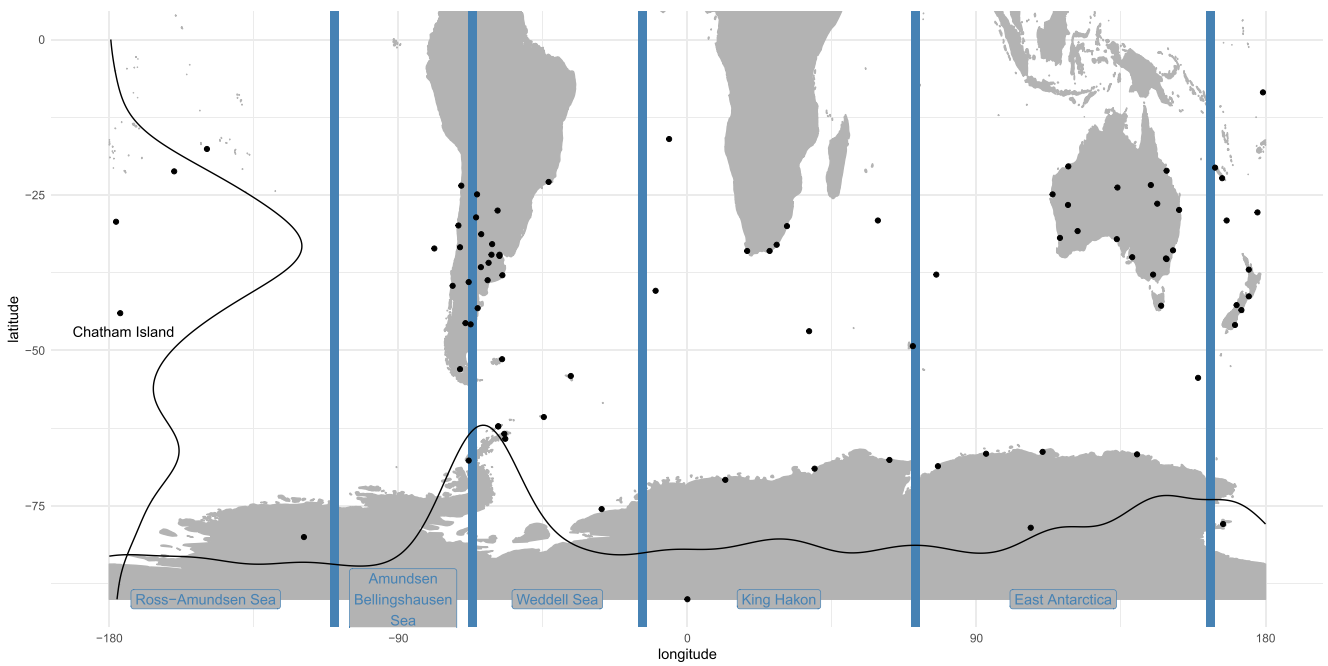

Figure 3. Location of weather stations collected by Fogt et al. (2016) and sea ice sectors defined in Raphael and Hobbs (2014). A density estimate of the stations' distribution over longitude and latitude is shown along the axes. A version of this figure with the station names is given in Figure S1.

Table 1
Covariance Matrix of Sea Ice Extent Anomaly in Mio. km² by Sector and in Total (Top) and Covariance Matrix of Error in Predicted Sea Ice Extent in Mio. km² by Sector and in Total (Bottom)

	Ross.A Sea	A.B. Sea	Weddell Sea	King H. VII	East Ant.	Total
Ross.A Sea	1.18	−0.11	−0.22	0.21	0.09	1.15
A.B. Sea	−0.11	0.29	−0.08	−0.13	−0.04	−0.08
Weddell Sea	−0.22	−0.08	0.93	−0.02	0.08	0.68
King H. VII	0.21	−0.13	−0.02	0.85	0.00	0.92
East Ant.	0.09	−0.04	0.08	0.00	0.32	0.44
Total	1.15	−0.08	0.68	0.92	0.44	3.12
	Ross.A Sea	A.B. Sea	Weddell Sea	King H. VII	East Ant.	Total
Ross.A Sea	1.06	−0.09	0.05	0.09	0.11	1.23
A.B. Sea	−0.09	0.23	−0.06	−0.06	−0.03	−0.01
Weddell Sea	0.05	−0.06	0.56	0.12	0.05	0.73
King H. VII	0.09	−0.06	0.12	0.76	0.03	0.94
East Ant.	0.11	−0.03	0.05	0.03	0.28	0.45
Total	1.23	−0.01	0.73	0.94	0.45	3.33

Note. Reported numbers are multiplied by a factor 10 to increase readability.

to a correlation matrix to preserve the scale of the variances and covariances, as the magnitude of sea ice variability varies notably among sectors. The variances on the diagonal measure the magnitude of the variability of the sea ice anomaly in each sector, with larger numbers implying higher variability. Even though the total sea ice anomaly is equal to the sum of the sea ice anomalies by sector, its variance is smaller than the sum of the variances by sector. Instead, the total sea ice anomaly's covariance with the sectors can be interpreted as their contribution to the total sea ice variability, in fact the sum of the covariances of each sector with the total is equal to the variance of the total. As an aside, this equality holds for an arbitrary number of sectors $Y_1, \ldots, Y_{N_Y}$ concatenated into an N_Y dimensional vector Y and their total sum $Y_\sum = \sum_s Y_s = \mathbf{1}^T Y$, as

$$\begin{aligned} \mathrm{Var}\left(Y_\sum\right) &= \mathrm{Var}\left(\mathbf{1}^T Y\right) \\ &= \mathrm{Cov}\left(\mathbf{1}^T Y, \mathbf{1}^T Y\right) \\ &= \mathbf{1}^T \mathrm{Cov}\left(Y, \mathbf{1}^T Y\right) \\ &= \sum_s \mathrm{Cov}\left(Y_s, \mathbf{1}^T Y\right) \\ &= \sum_s \mathrm{Cov}\left(Y_s, Y_\sum\right), \end{aligned} \tag{23}$$

where $\mathbf{1}$ denotes the vector of all ones of matching length.

3.2. Predictor Variables

As predictor variables in our model for Antarctic sea ice extent we use the data compiled by Fogt et al. (2016) from the University Corporation for Atmospheric Research data archive data set ds570000 (National Climatic Data Center, NESDIS, NOAA, U.S. Department of Commerce et al., 1981). Containing observations from 78 weather stations in the Southern hemisphere (see Figure 3) with a long measurement record for temperature (TMP) and SLP. These stations cluster heavily on Australia, South America, South Africa, and the Antarctic peninsula, with some island stations and stations on the Antarctic mainland.

Additionally, nine climate index reconstructions are collected in this data set. Note that during our reconstructions period these indices are reconstructions themselves, based on measurements of the exact same weather stations

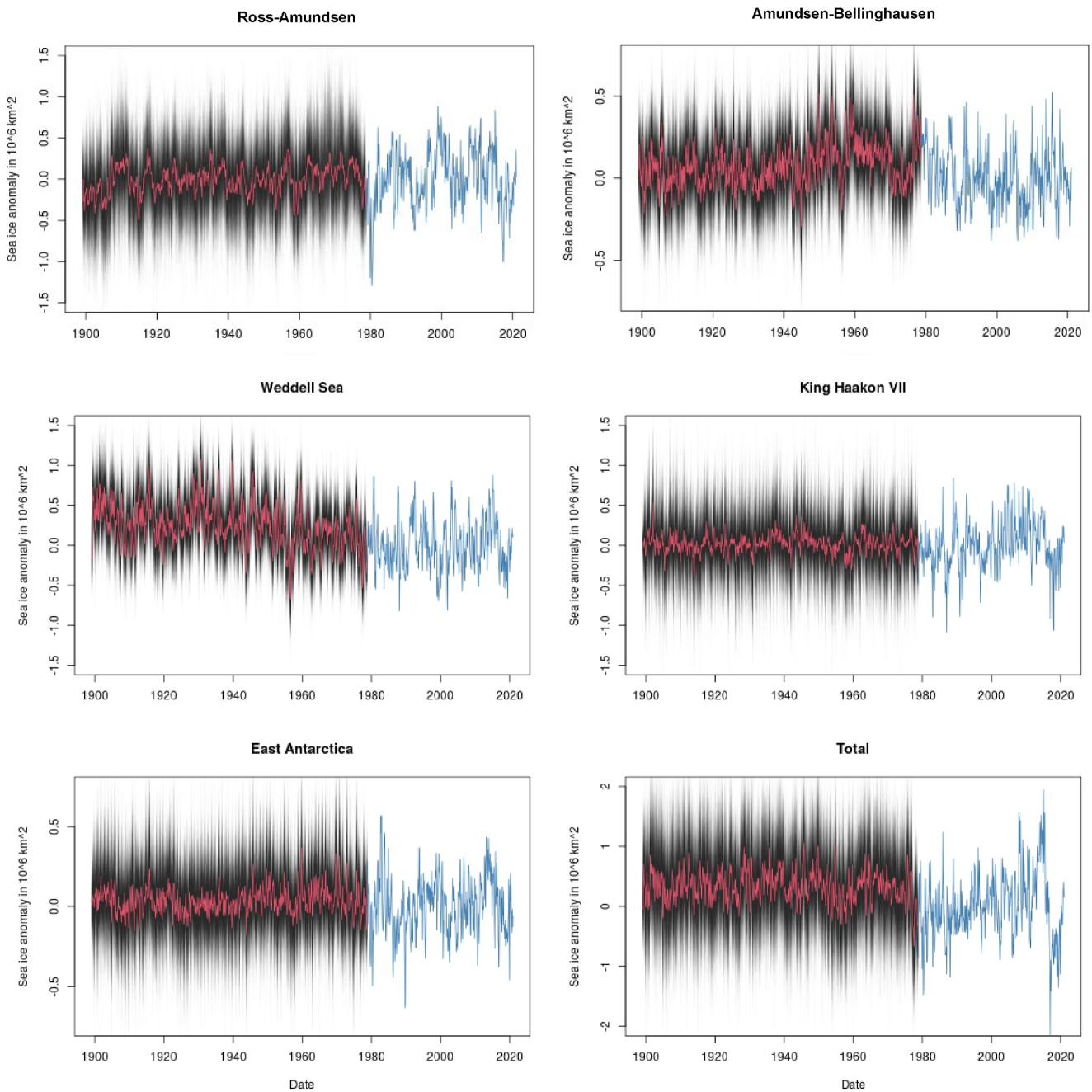

Figure 4. Ensemble reconstruction of 20th century Antarctic sea ice. The average reconstruction is drawn in red, the observed sea ice in blue, and the individual reconstructions light gray.

already included as predictor variables. This means, that these indices are (non-)linear transformations of the other covariates. Our model handles this potential collinearity effortlessly through harsh penalization of highly correlated predictor variables using horseshoe priors. A "double-counting" of stations does occur if a station is included as a predictor, and then again as part of a climate index based on its measurements, but this is not a problem for our model. A more severe form of "double-counting" occurs through geographical clustering of weather stations, in particular in Australia and South America. Geographically dense clusters of weather stations mean that the weather in this area is offered to the model multiple times without any added predictive value. To mitigate these effects we tried the use of (spatially weighted) empirical orthogonal functions (EOF) of the weather

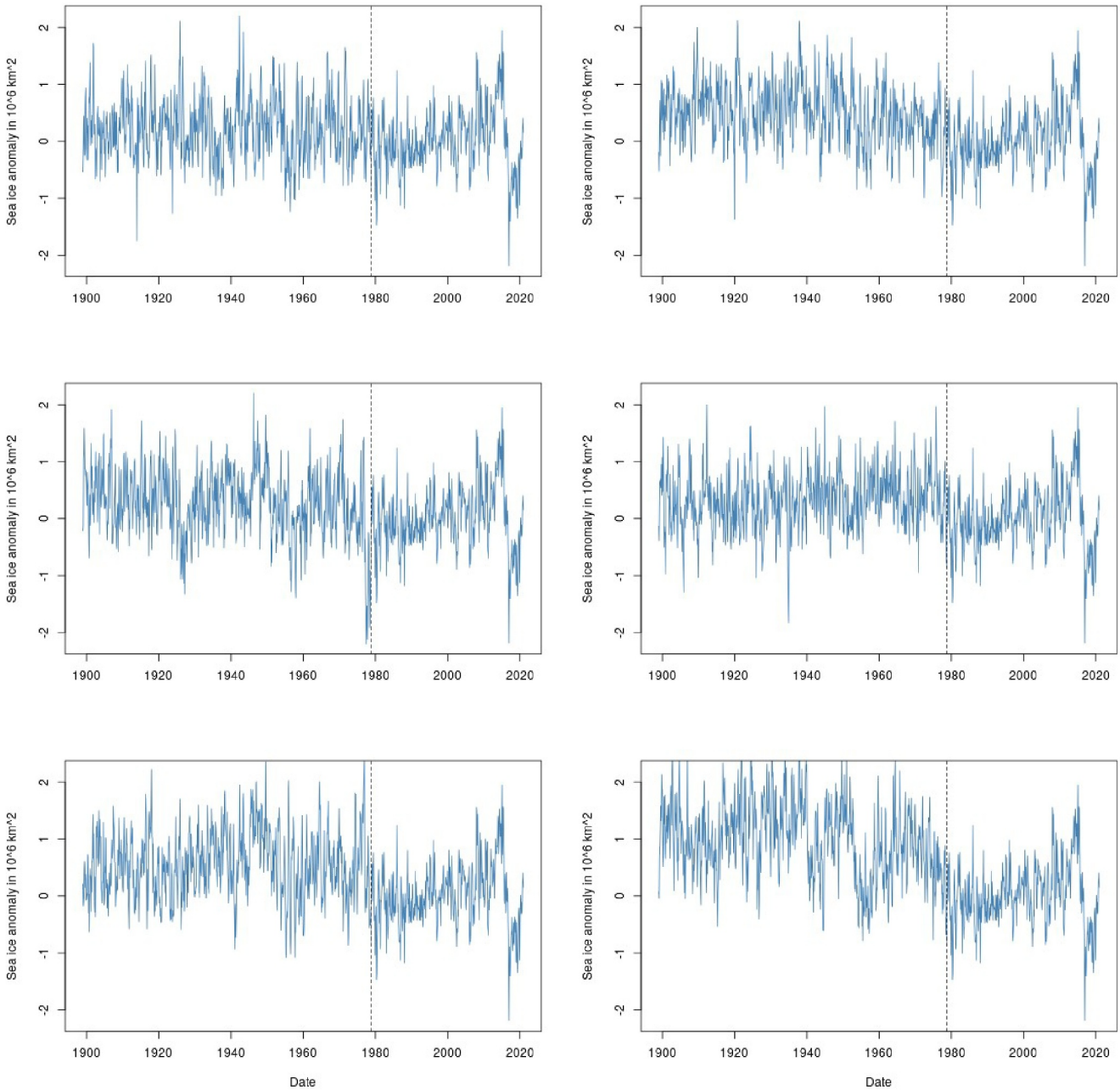

Figure 5. Individual reconstructions of 20th century total Antarctic sea ice. The dashed line separates reconstruction from observed data.

stations as predictors instead of the raw data, but found that our horseshoe priors are more effective at identifying predictive covariates and filtering out duplicate information.

The nine climate indices included are the northwest and southwest Pacific from the NOAA Extended Reconstructed Sea Surface Temperature data set, Version 5 (ERSST v5; B. Huang et al., 2015), the Pacific Decadal Oscillation (PDO; Mantua & Hare, 2002), four indices calculated from Niño SST from ERSSTv5 namely, the Niño 1 + 2 SSTs (averaged over 0°–10°S, 270°E − 280°E), the Niño 3 SSTs (5°N–5°S, 210°E–270°E), the Niño 3.4 SSTs (5°N–5°S, 190°E − 240°E) and the Niño 4 SSTs (5°N–5°S, 160°E−210°E), the Southern Oscillation Index (SOI; Australian Bureau of Meteorology, 2022), the Atlantic Multidecadal Oscillation (AMO; Enfield et al., 2001), the Southern Annular Mode index (SAM; Fogt & Marshall, 2020) merging the "Fogt" seasonal SAM index reconstructions (Fogt et al., 2009; Jones et al., 2009) which extend back to at least 1905 (http://polarmet.osu.edu/

ACD/sam/sam_recon.html) with the observation-based SAM index (Marshall, 2003) after 1957 (http://www.nerc-bas.ac.uk/icd/gjma/sam.html). All indices are available on a monthly scale, except for the SAM index which is only available seasonally and downsampled to monthly intervals by smooth interpolation. These indices describe large scale atmospheric and oceanic circulation patterns in the Southern Hemisphere that are known to influence Antarctic sea ice. Seven out of nine indices describe ocean variability, as the weather stations providing our other predictor data are land-based and geographically sparse.

4. Results

This section reports our model's reconstructions of 20th century Antarctic sea ice and describes their trends and variability. Our reconstructions display the previously established higher total sea ice extent in the first half of the 20th century than the second half, and match earlier Antarctic ice extent estimates obtained from direct satellite observations before 1980 well. We analyze our model by examining which weather stations it selects for reconstructing sea ice in which sector. Reassuringly, the model tends to select weather stations within or close to each sector and tends to focus on weather stations to the far South. We validate our model's predictive power internally using a cross validation.

4.1. Trends in 20th Century Antarctic Sea Ice Reconstructions

Here we give a brief overview of the trends and variability in Antarctic sea ice extent revealed by the reconstructed data. By the term trend we mean the conditional expectation of the sea ice extent as a function of time (i.e., it can be a non-linear function of time). Our ensemble of reconstructions is displayed in Figure 4 showing overplotted individual reconstructions (in black) and the overall reconstruction trend (in red) for all sectors and the total sea ice. The plots exhibit black vertical streaks in a pinstripe pattern due to the large difference in reconstruction uncertainty by month of year. The reconstruction uncertainty is highest during the sea ice melt season, lower during the sea ice growth season, even lower close to the maximal sea ice, and lowest during the low sea ice season. This can be seen in detail in Figure 6, showing the ensemble reconstruction for February 1977–February 1978. The trend in reconstructed total sea ice is the sum of all trends in all sectors, as the total sea ice is computed as the sum of sea ice in all sectors. The large trends in the Weddell Sea and Amundsen-Bellingshausen Sea sectors, and the smaller contrasting trend in the Ross-Amundsen Sea sector sum out to an overall higher level of reconstructed total Antarctic sea ice in comparison with the satellite observed period, and a sharp decline in Antarctic sea ice in the 1970s. To show the variability within and between individual reconstructions a set of six randomly picked individual reconstructions of the total sea ice are showcased in Figure 5. Each of these six individual reconstructions is an equally likely depiction of a possible evolution of Antarctic sea ice extent in the 20th century. Their variability patterns matches the satellite record on small as well as large time scales so accurately, that the reconstruction period is indistinguishable from the satellite observed period by eye.

4.2. Comparison With Early Satellite Observations

For a few months in our reconstruction period direct satellite observations of the Southern Hemisphere exist that have been analyzed manually by Meier et al. (2013) and Gallaher et al. (2014) to obtain estimates of Antarctic sea ice extent. This is a difficult and labor intensive task, as these images are taken in the visible spectrum and the sea ice edge is obscured by a 40%–90% cloud cover depending on season and location. In every satellite image, observed fractions of the sea ice edge are manually identified, grouped by month and then manually compiled into a complete sea ice edge. This process accrues multiple sources of uncertainty but nonetheless gives a reasonably good estimate of historical sea ice extent. Table 2 shows the mean and standard error of the estimated total sea ice anomaly for the satellite observed sea ice and our reconstruction. For September 1964 and May through July 1966 we find good agreement between our reconstruction and the satellite observed sea ice, with our reconstructed average always being smaller in magnitude. This damper effect can be explained by the regularization scheme of our method which brings all regression coefficients and thus average predictions closer to zero in order to increase stability. Note that the variability of individual reconstructions is not dampened by our regularization scheme as error terms are unpenalized. This means that extreme events at the monthly level are created true to the internal variability. The reliability of the reconstruction for August 1966 created by Gallaher et al. (2014) has been

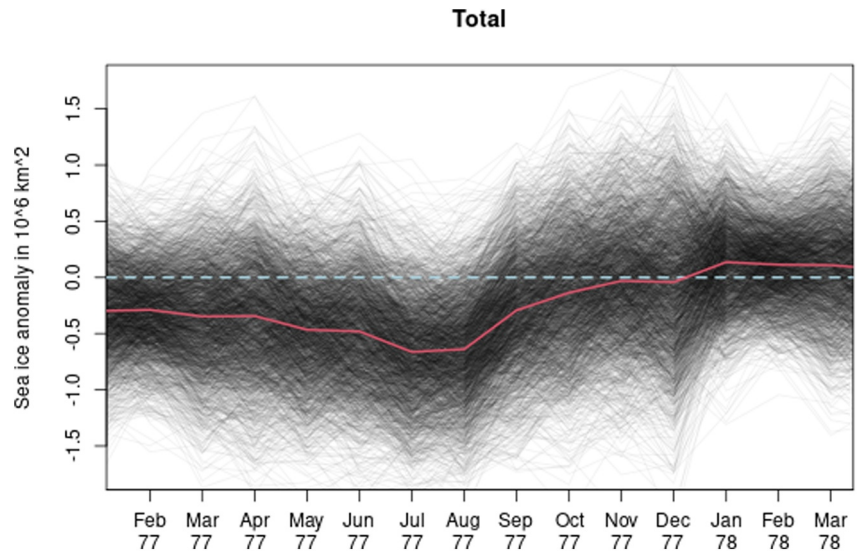

Figure 6. Ensemble reconstruction of total Antarctic sea ice anomaly from February 1977 to February 1978. Individual reconstructions are drawn in light gray and the average reconstruction in red.

questioned by the authors themselves due to missing values in that month. A decrease in sea ice anomaly was deemed plausible in this month, but probably not at that magnitude.

As a quantitative measure of the agreement between the satellite observed reconstruction and our reconstruction, we compute the Kullback-Leibler divergence (KL divergence; Kullback & Leibler, 1951), a distance metric between distributions p_1 and p_2, given as

$$\begin{aligned} D_{\mathrm{KL}}(p_1 \| p_2) &= \mathbb{E}_{p_1}\left[\log \frac{p_1(x)}{p_2(x)}\right] \\ &= \int_x \log \frac{p_1(x)}{p_2(x)} p_1(x) \partial x \end{aligned} \tag{24}$$

between the sea ice anomaly distributions produced by the satellite observed reconstruction and our reconstruction. For practical reasons, we assume both the satellite observed reconstruction and our reconstruction for a given month follow a Gaussian distribution using the mean and standard deviation given in Table 2; not an unreasonable assumption since the distribution of the satellite observed reconstructions is unknown and our reconstructions follow the typical bell shaped distribution seen in Gaussian distributions. This distribution assumption of Gaussianality works in our favor by allowing the use of the closed form solution for the KL

Table 2
Average (Mean) and Standard Error (Se) of Estimated Sea Ice Anomaly From Direct Satellite Observation (Sat.) and Our Reconstruction (Rec.)

Month	Sat. Mean	Sat. Se	Rec. Mean	Rec. Se	2 × KL	*p*-val
September 1964	0.90	0.40[a]	0.75	0.56	0.41	0.82
May 1966	0.40	0.20	0.50	0.52	4.09	0.13
June 1966	1.00	0.40	0.50	0.53	1.76	0.41
July 1966	0.60	0.50	0.47	0.51	0.07	0.97
August 1966	−1.60[b]	0.40[b]	0.55	0.51	28.89	0.00

Note. We also report two times the Kullback Leibler divergence (2 × KL) between the two distributions and its *p*-value (*p*-val) in a Chi-square distribution with 2° of freedom. [a]We compute the standard error by treating the range given in Meier et al. (2013) as a 95% confidence interval in a Gaussian distribution. [b]This estimate is seriously doubted by the authors due to missing observations.

divergence for Gaussian distributed random variables $X_1 \sim p_1 = N(\mu_1, \sigma_1^2)$, $X_2 \sim p_2 = N(\mu_2, \sigma_2^2)$ which can be derived to be

$$\mathrm{KL}(p_1 \| p_2) = \log \frac{\sigma_2}{\sigma_1} + \frac{\sigma_1^2 + (\mu_1 - \mu_2)^2}{2\sigma_2^2} - \frac{1}{2}. \tag{25}$$

large values in KL divergence imply a larger difference in distributions, but in order to interpret the scale of these divergences, we use the statistical relation that $2 \times n_0$ times the KL divergence between a distribution with m_0 estimated parameters and the same distribution with fixed reference parameters approximately follows a Chi-square distribution with $m_0{}^\circ$ of freedom (e.g., Belov & Armstrong, 2011),

$$2n_0 D_{\mathrm{KL}}(p_1 \| p_2) \overset{\text{approx.}}{\sim} \chi^2_{m_0}, \tag{26}$$

where n_0 is the number of observations on which the parameters were estimated. In our case, we compare a Gaussian distribution with estimated mean and standard deviation $(m_0 = 2)$ for 1 month $(n_0 = 1)$ to a Gaussian distribution with parameters given by Meier et al. (2013) and Gallaher et al. (2014), so 2×1 times the computed KL divergence approximately follows a Chi-square distribution with 2° of freedom. This distribution approximation allows us the computation of p-values testing the null hypothesis "H_0: Our reconstruction follows the same distribution as the satellite observed reconstruction" versus the alternative hypothesis "H_1: Our reconstruction does not follow the same distribution as the satellite observed reconstruction." This confirms that only for August 1966 does our reconstruction differs significantly from the satellite observed reconstructions created by Meier et al. (2013) and Gallaher et al. (2014).

4.3. Importance of Individual Weather Stations

Figure 7 shows the importance of individual stations in the sea ice reconstruction. For each sector, the importance of a station is measured as the sum of the magnitudes of all regression coefficients relating to measurements of this station, that is, the sum of the absolute values of the regression coefficients for the station's temperature and SLP measurements and lags thereof. We notice that our model heavily relies on measurements from stations within the same sector for sea ice reconstruction, in particular for the Weddell Sea, King Haakon VII Sea, and East Antarctica sectors. Note the lack of weather stations in the Ross-Amundsen Sea sector itself predicting Amundsen-Ross Sea sector sea ice extent due to the nonexistence of stations in this sector South of the Chatham island station at 44° South, see Figure 3 showing the location of all stations in our data. This probably contributes to relatively low predictive power of our model in this sector. There is also a lack of stations in the Amundsen-Bellingshausen Sea sector, with stations in this sector mainly on the South American mainland, see Figure 3, but our model still achieves a good reconstruction using nearby stations.

4.4. Predictive Performance

We perform a leave-one-out cross validation (LOOCV, e.g., Celisse, 2014) to estimate the predictive performance of our model. In a traditional LOOCV one observation is left out of the data set and predicted using a model fit on the remainder of the data. This process is repeated for every observation in the data resulting in a prediction associated with every observation. These predictions are then compared to the known true observation to obtain measures of model performance. Following Fogt et al. (2022), we do not only leave out the data of the 1 month we are trying to predict, but also all data from its year and the 2 years before and after, resulting in 42–5 = 37 years of training data for each model. This is necessary due to the autocorrelated nature of the data set and our model. This process creates a set of validation reconstructions, whose average prediction per month and sector is compared to the climatology. We also perform the same cross validation on the climatology, computing the climatological mean using only those years not left out. For our average validation reconstruction and our climatology we compute the correlation, coefficient of efficiency (CE; Cook et al., 1999), and root mean squared error (RMSE) with the true observed sea ice by sector, see Table 3. Correlations are bound between $[-1, 1]$ and higher values imply better performance, the CE is bound between $[-\infty, 1]$ and higher values imply better performance, the average error (AE) is bound between $[0, \infty]$ and lower values imply better performance, and the RMSE is bound between $[0, \infty]$ and lower values imply

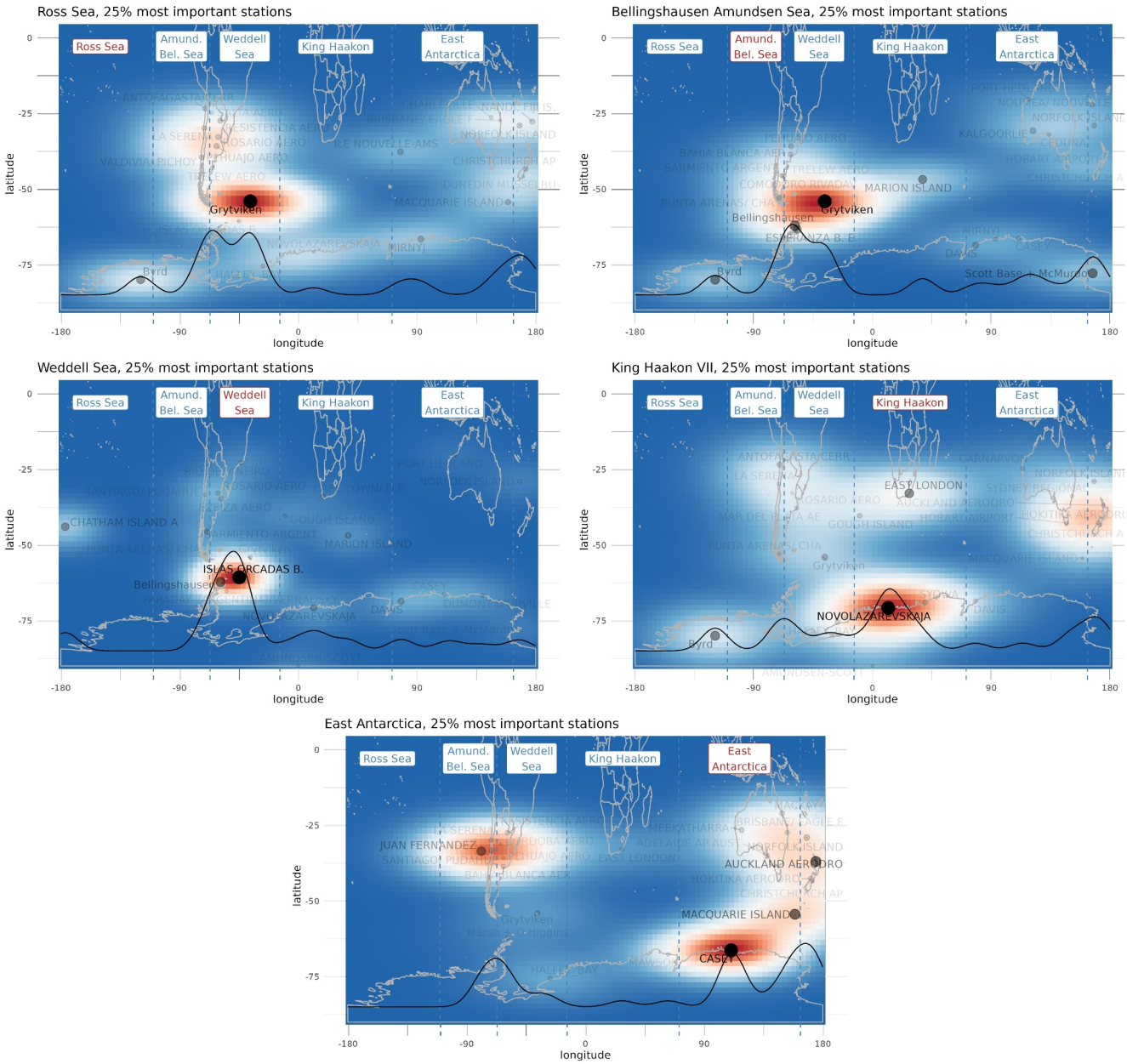

Figure 7. Importance of weather station in sea ice reconstruction by sector. A station's importance is measured as the sum of the absolute values of all regression coefficients pertaining to its data.

better performance. Note that "almost by design" the climatology has a negative correlation and CE with the ground truth. When computing the climatological mean on detrended data, the climatological mean is always exactly zero. When computing the climatological mean on detrended data where a few years are left out, it will shift in the opposite direction of the anomaly in the left out years. Our model's sea ice predictions for the Ross-Amundsen Sea, King Haakon VII Sea, and East Antarctica sectors, have a moderate correlation with the observed sea ice values, strong correlation for the Amundsen-Bellingshausen Sea and Weddell Sea sectors, but only a weak positive correlation with the total sea ice. The two other measures of skill, mean absolute error and root mean square error, both show improvements of our model over climatology. In all cases the intrinsic variation in sea ice extent values is substantial. The lack of a stronger correlation for the total sea ice is surprising, as the predicted total sea ice is

Table 3
Performance of Our Model (Mod) and the Climatology (Cli) in the LOOCV

Sector	cor cli	cor mod	ce cli	ce mod	mae cli	mae mod	rmse cli	rmse mod
Ross.A Sea	−0.51	0.34	−0.05	0.08	0.28	0.25	0.35	0.33
A.B. Sea	−0.26	0.57	−0.04	0.32	*0.14*	0.11	0.17	0.14
W. Sea	−0.17	0.65	−0.04	0.42	0.25	0.18	0.31	0.23
K.H. VII	−0.31	0.38	−0.05	0.13	0.22	0.21	0.30	0.27
E. Ant.	−0.06	0.30	−0.03	0.03	0.14	0.14	0.18	0.17
Total	−0.45	*0.08*	−0.05	*−0.13*	0.44	0.44	0.57	0.59

Note. We compare the correlation coefficient (cor), coefficient of efficiency (ce), mean absolute error (mae), and root mean squared error (rmse). The three values that are not statistically significant at the 5% level are marked in italic.

computed as the sum of the predictions for each sector. The bottom half of Table 1, showing the covariance matrix of prediction errors, offers some insight into this. The covariance among all sectors is positive. The only exception is the Amundsen-Bellingshausen Sea sector, where the errors are negatively correlated with errors in all other sectors. This means, that with the exception of the Amundsen-Bellingshausen Sea sector, our model tends to make the same kind of error simultaneously in all sectors, that is, we tend to predict too much or too little sea ice in all sectors at the same time. This in turn implies that the total sea ice will be predicted even more incorrectly, as the errors in the sectors tend to sum up, instead of canceling each other out. This makes prediction errors in the total larger than in any individual sector. With the same statistical reasoning as for the covariance matrix reported in the top of Table 1, we can interpret the covariance between the errors by sector with the error in total sea ice (last row and last column of the bottom half of Table 1) as their contribution to the total error. Furthermore, as the scale of the sea ice anomalies underlying the top half of Table 1 and sea ice prediction error underlying the bottom half of Table 1 is the same, their numerical values can be compared directly. This reveals, that while the variances in prediction errors are smaller than the variances in sea ice anomalies in every sector, their contributions to (covariances with) the total prediction error are larger. This leads to a larger variance in prediction error for the total sea ice than variance in total sea ice anomaly.

The performance of our model over time is shown in Figure 8, showing the predictions on holdout data in our LOOCV for every month in our data set. The average reconstruction on holdout data is plotted in red, the true observed sea ice in blue. The good numerical performance of our reconstruction model in the Amundsen-Bellingshausen Sea and Weddell Sea sectors manifests itself in the good visual agreement between the average reconstruction (in red) and the true sea ice (in blue) in these sectors. Our model fails to replicate the 2014–2017 decline in total Antarctic sea ice and relevant sectors, with the observed total sea ice at the margin of our reconstruction uncertainty. Two main explanations come to mind, either the relationship between Antarctic sea ice and Southern Hemisphere weather has changed, or an unobserved driver not captured in our covariates has caused the dramatic decline. Our model's failure to replicate this dramatic sea ice decline highlights the fact that this occurrence is highly unusual.

4.5. Impact of Station Distribution and Time on Predictive Performance

The lack of stations in certain sectors may contribute to lower predictive performance and higher variation in the reconstruction. However, the model and the reconstructions both adjust to the available information. Specifically, low information about a sector is expressed by higher variation in sea ice reconstructed values between ensemble members in that sector. Hence the accuracy and robustness can be measured by, for example, the standard deviations in the reconstruction in each sector. Table 4 reports the standard deviations for each sector during the early 20th century, the pre-satellite era and the satellite era. We see that the variation is modestly increased the further back in time the reconstructions are from the satellite era. They also vary by sector. The Ross-Amundsen and Weddell Seas sectors have high variation while the Amundsen-Bellingshausen Sea and East Antarctica sectors have lower values. These values reflect both the intrinsic variation in the sea ice extent and the information

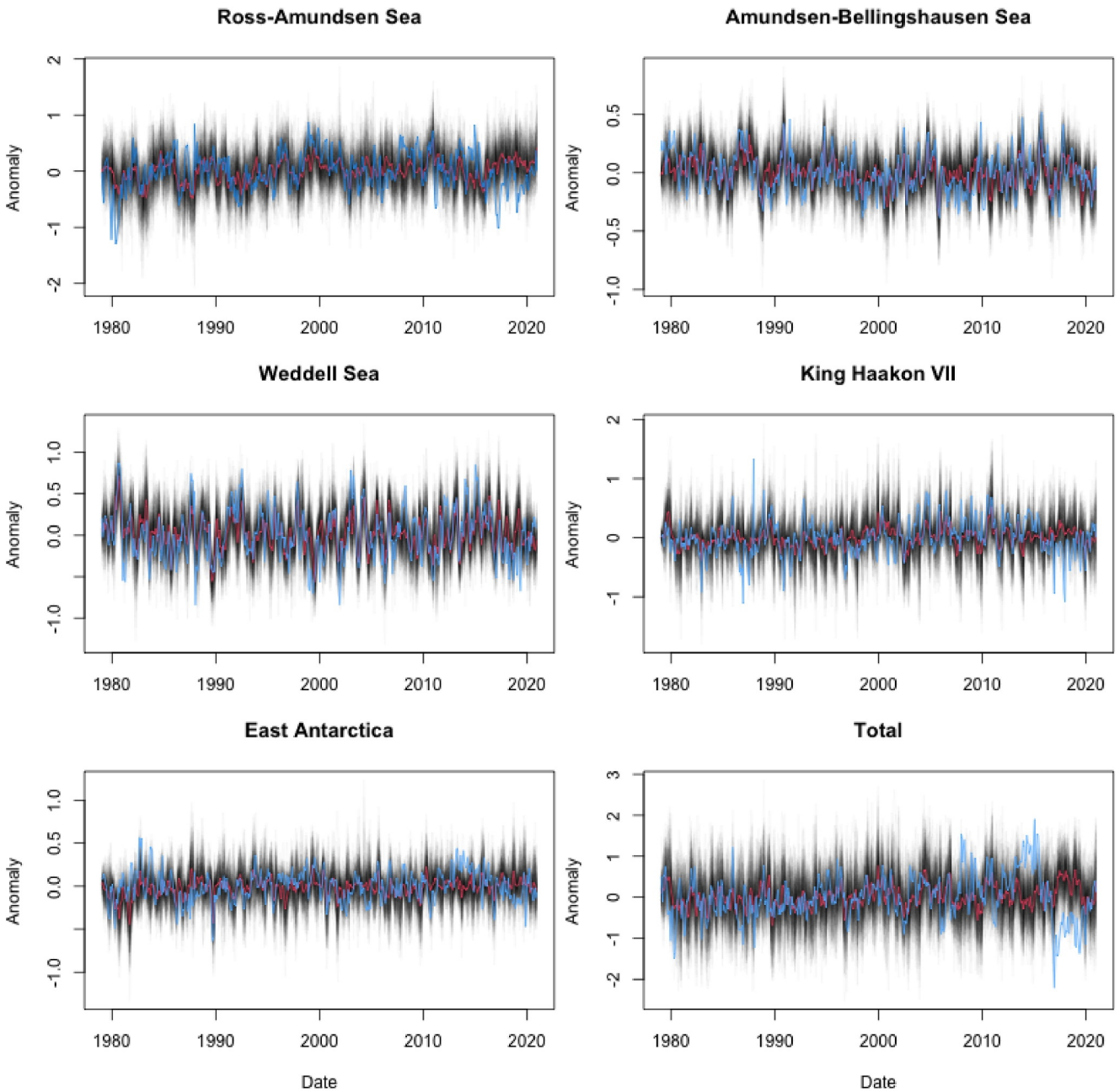

Figure 8. Out of sample reconstruction in the LOOCV. Individual reconstructions are drawn in light gray, the average reconstruction in red, the true sea ice in blue.

we have on them. In terms of potential strategies for addressing the lack of stations in certain sectors, we note that our model makes what we believe is an accurate reconstruction given the available information. As such, statistical model improvements are unlikely to improve the quality of the reconstructions. A natural way to improve the accuracy of the reconstruction is to bring more information to bear, be it either empirical or climate model or both.

Table 4
Variation in Sea Ice Extent Reconstructions by Period and Sector

Sector	Complete 1900–2020	Early 20th century 1900–1950	Pre-satellite era 1951–1978	Satellite era 1979–2020
Ross.A Sea	0.349	0.340	0.343	0.343
A.B. Sea	0.185	0.172	0.188	0.173
W. Sea	0.326	0.313	0.307	0.286
K.H. VII	0.294	0.283	0.287	0.300
E. Ant.	0.188	0.182	0.188	0.183
Total	0.501	0.521	0.509	0.474

5. Conclusions

We present the first complete monthly time series reconstruction of Antarctic sea ice for the 20th century. We provide a set of 2,500 reconstructions of Antarctic sea ice by sector and in total, with realistic month-to-month progression, sector-to-sector covariability, and total sea ice extent variability. This is achieved by the introduction of a seasonal VARMA model that we fit in a Bayesian framework. Our model draws its realism from formulating a joint time series model for all sectors (VARMA) which creates plausible month-to-month progression and sector-to-sector covariability resulting in plausible total sea ice extent variability. The Bayesian framework naturally creates and ensemble of reconstructions as posterior draws from the joint distribution of the unobserved sea ice extent from 1900 to 1978 for all sectors. We validate our method internally using a LOOCV, showing predictive power particularly in the Amundsen-Bellingshausen Sea, Weddell Sea, and the Ross-Amundsen Sea, King Haakon VII Sea, and East Antarctica sectors to a lesser degree. The overall sea ice is not reconstructed better than by a climatology, but our reconstructions contain realistic variability as well as spatio-temporal autocorrelation patterns not contained in the climatology. For many applications the use of a climatology will result in dramatic underestimation of uncertainty due to lack of variability in sea ice anomalies. A further reassurance of the validity of our model is the geographic distribution of weather stations deemed important for sea ice reconstruction by sector. Stations with high importance tend to cluster within or nearby the reconstructed sector. Our method is externally validated by high agreement with the sea ice reconstructions created for September 1964 (Meier et al., 2013) and May–August 1966 (Gallaher et al., 2014) based on direct satellite observations.

This paper invites a wide array of new research opportunities. Dirichlet autoregressive moving-average model as introduced in Katz et al. (2024) are another promising approach for modeling Antarctic sea ice extent in the framework of Bayesian time series analysis. Instead of creating a multivariate model for sea ice extent in all sectors and the total sea ice extent reconstructed as the sum of all sectors, a Dirichlet model reconstructs the total sea ice extent and then models its distribution across the sectors. We chose our multivariate approach over the Dirichlet approach because it is more intuitive and somewhat simpler in its implementation. Including a temporal and spatial autoregressive component as well as sparsity inducing priors, our model's statistical building blocks are probably close to optimal; more work can be done on hyper-parameter tuning and model selection. Our choice of which order of autoregressive parameters to include as well as the strength of our sparsity prior are chosen based on expert knowledge but might be improved using more rigorous statistical methods.

Collecting more covariates, and in particular more powerful covariates is certainly fruitful endeavor for future research that will probably have the biggest impact on reconstruction accuracy. One promising source is ice core data (Thomas & Abram, 2016; Thomas et al., 2019). A strength of our method is that it provides a framework to combine disparate types of information. In particular, ice core salt or MSA concentrations can be included as X_t variables in Equation 3. In many cases the temporal scale of the ice core proxies will be larger than monthly, but these can be included as multiple variables to reflect the aggregation effects.

An exciting extension of our work made possible by its Bayesian formulation is the possibility of using prior information in the form of direct sea ice observations to improve reconstruction accuracy. In this application, we can think of prior distributions as containing outside information that can be used to increase the model precision. If we were to use the early satellite observations analyzed by Meier et al. (2013) and Gallaher et al. (2014) as prior information for sea ice extent, our model posterior reconstructions would be something like a weighted average with reduced standard error between the satellite based reconstruction and our current reconstruction. In addition to the early satellite observations analyzed by Meier et al. (2013) and Gallaher et al. (2014), a vast amount of information about early 20th century Antarctic sea ice remains hidden in ship log books (e.g., Edinburgh & Day, 2016). These contain notes of direct sea ice observations at a certain date and location. This information can be related to a (local) sea ice edge or (local) sea ice extent using a to-date nonexistent statistical model, which will result in prior information for (local) sea ice extent reconstruction. This method should obtain useful priors for the sea ice all they way back to the beginning of the 20th century.

These priors "anchor" the reconstructions and are expected to lead to dramatic reductions in reconstruction uncertainty. Preliminary analysis using the direct satellite observations reported in Meier et al. (2013) and Gallaher et al. (2014) show promising results in reducing reconstruction uncertainty in months with available prior information as well as neighboring months.

An exciting prospect is the use of our set of reconstructions in further scientific explorations. We envision the use of these reconstructions to analyze extreme events that were observed during the satellite period in the broader historical context of the entire 20th century. Our reconstructions can also be used to calibrate climate models; using our reconstructions as opposed to the climatology will ensure plausible trends and variability in historical levels of Antarctic sea ice extent.

Data Availability Statement

The Antarctic sea ice concentration data is publicly available from the website of the National Snow and Ice Data Center (NSIDC). We used the climate data record (CDR) daily concentration fields from the NOAA/NSIDC CDR of Passive Microwave Sea Ice Concentration, Version 4 (https://nsidc.org/data/g02202; Meier et al., 2016). The predictor variables for our model are the data compiled by Fogt et al. (2016) from the University Corporation for Atmospheric Research data archive data set ds570000 (National Climatic Data Center, NESDIS, NOAA, U.S. Department of Commerce et al., 1981).

The code used to compute the sea ice extent, create the reconstruction model for the sea ice extent, and create all figures and tables, is published openly online (Maierhofer, 2024). The complete set of reconstructions can be downloaded from Maierhofer (2023).

Acknowledgments
This work was supported by the National Science Foundation (NSF) under the Office of Polar Programs under Grant NSF-OPP-1745089.

References

Abram, N. J., Mulvaney, R., & Arrowsmith, C. (2011). Environmental signals in a highly resolved ice core from James Ross Island, Antarctica. *Journal of Geophysical Research*, *116*(20), 1–15. https://doi.org/10.1029/2011JD016147

Abram, N. J., Thomas, E. R., McConnell, J. R., Mulvaney, R., Bracegirdle, T. J., Sime, L. C., & Aristarain, A. J. (2010). Ice core evidence for a 20th century decline of sea ice in the Bellingshausen Sea, Antarctica. *Journal of Geophysical Research*, *115*(23), 1–9. https://doi.org/10.1029/2010JD014644

Abram, N. J., Wolff, E. W., & Curran, M. A. (2013). A review of sea ice Proxy information from polar ice cores. *Quaternary Science Reviews*, *79*, 168–183. https://doi.org/10.1016/j.quascirev.2013.01.011

Australian Bureau of Meteorology. (2022). Southern Oscillation Index (SOI) since 1876. Retrieved from http://www.bom.gov.au/climate/enso/soi/

Becagli, S., Castellano, E., Cerri, O., Curran, M., Frezzotti, M., Marino, F., et al. (2009). Methanesulphonic Acid (MSA) stratigraphy from a Talos Dome ice core as a tool in depicting sea ice changes and southern atmospheric circulation over the previous 140 years. *Atmospheric Environment*, *43*(5), 1051–1058. https://doi.org/10.1016/j.atmosenv.2008.11.015

Belov, D. I., & Armstrong, R. D. (2011). Distributions of the Kullback–Leibler divergence with applications. *British Journal of Mathematical and Statistical Psychology*, *64*(2), 291–309. https://doi.org/10.1348/000711010x522227

Brady, E., Stevenson, S., Bailey, D., Liu, Z., Noone, D., Nusbaumer, J., et al. (2019). The connected isotopic water cycle in the community earth system model version 1. *Journal of Advances in Modeling Earth Systems*, *11*(8), 2547–2566. https://doi.org/10.1029/2019ms001663

Carvalho, C. M., Polson, N. G., & Scott, J. G. (2010). The horseshoe estimator for sparse signals. *Biometrika*, *97*(2), 465–480. https://doi.org/10.1093/biomet/asq017

Celisse, A. (2014). Optimal cross-validation in density estimation with the L2-loss. *Annals of Statistics*, *42*(5), 1879–1910. https://doi.org/10.1214/14-aos1240

Cook, E. R., Meko, D. M., Stahle, D. W., & Cleaveland, M. K. (1999). Drought reconstructions for the continental United States. *Journal of Climate*, *12*(4), 1145–1162. https://doi.org/10.1175/1520-0442(1999)012<1145:drftcu>2.0.co;2

Cotté, C., & Guinet, C. (2007). Historical whaling records reveal major regional retreat of Antarctic sea ice. *Deep-Sea Research Part I Oceanographic Research Papers*, *54*(2), 243–252. https://doi.org/10.1016/j.dsr.2006.11.001

Curran, M. A., van Ommen, T. D., Morgan, V. I., Phillips, K. L., & Palmer, A. S. (2003). Ice core evidence for Antarctic Sea Ice decline since the 1950s. *Science*, *302*(5648), 1203–1206. https://doi.org/10.1126/science.1087888

Dalaiden, Q., Goosse, H., Rezsöhazy, J., & Thomas, E. R. (2021). Reconstructing atmospheric circulation and sea-ice extent in the West Antarctic over the past 200 years using data assimilation. *Climate Dynamics*, *57*(11–12), 3479–3503. https://doi.org/10.1007/s00382-021-05879-6

De la Mare, W. K. (1997). Abrupt mid-twentieth-century decline in Antarctic sea-ice extent from whaling records. *Nature*, *389*(6646), 57–60. https://doi.org/10.1038/37956

De La Mare, W. K. (2009). Changes in Antarctic sea-ice extent from direct historical observations and whaling records. *Climatic Change*, *92*(3–4), 461–493. https://doi.org/10.1007/s10584-008-9473-2

Edinburgh, T., & Day, J. J. (2016). Estimating the extent of Antarctic summer sea ice during the heroic age of Antarctic exploration. *The Cryosphere*, *10*(6), 2721–2730. https://doi.org/10.5194/tc1027212016

Enfield, D. B., Mestas-Nuñez, A. M., & Trimble, P. J. (2001). The Atlantic Multidecadal oscillation and its relation to rainfall and river flows in the continental us. *Geophysical Research Letters*, *28*(10), 2077–2080. https://doi.org/10.1029/2000gl012745

Fogt, R. L., Jones, J. M., Goergens, C. A., Jones, M. E., Witte, G. A., & Lee, M. Y. (2016). Antarctic station-based seasonal pressure reconstructions since 1905: 2. Variability and trends during the twentieth century. *Journal of Geophysical Research*, *121*(6), 2836–2856. https://doi.org/10.1002/2015JD024565

Fogt, R. L., & Marshall, G. J. (2020). The southern annular mode: Variability, trends, and climate impacts across the southern hemisphere. *Wiley Interdisciplinary Reviews: Climate Change*, *11*(4), e652. https://doi.org/10.1002/wcc.652

Fogt, R. L., Perlwitz, J., Monaghan, A. J., Bromwich, D. H., Jones, J. M., & Marshall, G. J. (2009). Historical SAM variability. Part II: Twentieth-century variability and trends from reconstructions, observations, and the IPCC AR4 models. *Journal of Climate*, *22*(20), 5346–5365. https://doi.org/10.1175/2009jcli2786.1

Fogt, R. L., Sleinkofer, A. M., Raphael, M. N., & Handcock, M. S. (2022). A regime shift in seasonal total Antarctic sea ice extent in the twentieth century. *Nature Climate Change*, *12*(1), 54–62. https://doi.org/10.1038/s41558-021-01254-9

Gallaher, D. W., Campbell, G. G., & Meier, W. N. (2014). Anomalous variability in Antarctic sea ice extents during the 1960s with the use of Nimbus data. *IEEE Journal of Selected Topics in Applied Earth Observations and Remote Sensing*, *7*(3), 1116–1122. https://doi.org/10.1109/JSTARS.2013.2264391

Gelman, A., Carlin, J. B., Stern, H. S., & Rubin, D. B. (2004). *Bayesian data analysis*. Chapman and Hall/CRC.

Handcock, M. S., & Raphael, M. N. (2020). Modeling the annual cycle of daily Antarctic sea ice extent. *The Cryosphere*, *14*(7), 2159–2172. https://doi.org/10.5194/tc-14-2159-2020

Hobbs, W., Curran, M., Abram, N., & Thomas, E. R. (2016). Century-scale perspectives on observed and simulated Southern Ocean sea ice trends from proxy reconstructions. *Journal of Geophysical Research: Oceans*, *121*(10), 7804–7818. https://doi.org/10.1002/2016JC012111

Hobbs, W. R., Bindoff, N. L., & Raphael, M. N. (2015). New perspectives on observed and simulated Antarctic sea ice extent trends using optimal fingerprinting techniques. *Journal of Climate*, *28*(4), 1543–1560. https://doi.org/10.1175/jcli-d-14-00367.1

Huang, B., Banzon, V. F., Freeman, E., Lawrimore, J., Liu, W., Peterson, T. C., et al. (2015). Extended Reconstructed Sea Surface Temperature Version 4 (ERSST v4). Part I: Upgrades and intercomparisons. *Journal of Climate*, *28*(3), 911–930. https://doi.org/10.1175/jcli-d-14-00006.1

Huang, H. C., & Cressie, N. (1996). Spatio-temporal prediction of snow water equivalent using the Kalman Filter. *Computational Statistics & Data Analysis*, *22*(2), 159–175. https://doi.org/10.1016/0167-9473(95)00047-x

Jones, J. M., Fogt, R. L., Widmann, M., Marshall, G. J., Jones, P. D., & Visbeck, M. (2009). Historical SAM variability. Part I: Century-length seasonal reconstructions. *Journal of Climate*, *22*(20), 5319–5345. https://doi.org/10.1175/2009jcli2785.1

Katz, H., Brusch, K., & Weiss, R. E. (2024). A Bayesian Dirichlet auto-regressive moving average model for forecasting lead times. *International Journal of Forecasting*, *40*(4), 1556–1567. https://doi.org/10.1016/j.ijforecast.2024.01.004

Krawczyk, D. W., Witkowski, A., Moros, M., Lloyd, J. M., Høyer, J. L., Miettinen, A., & Kuijpers, A. (2017). Quantitative reconstruction of Holocene sea ice and sea surface temperature off West Greenland from the first regional diatom data set. *Paleoceanography*, *32*(1), 18–40. https://doi.org/10.1002/2016PA003003

Kullback, S., & Leibler, R. A. (1951). On information and sufficiency. *The Annals of Mathematical Statistics*, *22*(1), 79–86. https://doi.org/10.1214/aoms/1177729694

Maierhofer, T. J. (2023). 20th Century Antarctic sea ice extent anomaly reconstruction by sector. *Zenodo*. https://doi.org/10.5281/zenodo.7971734

Maierhofer, T. J. (2024). Software to reconstruct the 20th century Antarctic sea ice extent by sector. *GitHub*. Retrieved from https://github.com/maierhofert/AntarcticSeaIce/tree/main/ExtentReconstruction

Mantua, N. J., & Hare, S. R. (2002). The pacific decadal oscillation. *Journal of Oceanography*, *58*(1), 35–44. https://doi.org/10.1023/a:1015820616384

Marshall, G. J. (2003). Trends in the southern annular mode from observations and reanalyses. *Journal of Climate*, *16*(24), 4134–4143. https://doi.org/10.1175/1520-0442(2003)016<4134:titsam>2.0.co;2

Meier, W. N., Fetterer, F., Windnagel, A. K., & Stewart, J. S. (2016). NOAA/NSIDC climate data record of passive Microwave Sea Ice concentration, version 4. https://doi.org/10.7265/efmz-2t65

Meier, W. N., Gallaher, D., & Campbell, G. G. (2013). New estimates of Arctic and Antarctic sea ice extent during September 1964 from recovered Nimbus I satellite imagery. *The Cryosphere*, *7*(2), 699–705. https://doi.org/10.5194/tc-7-699-2013

Meyerson, E. A., Mayewski, P. A., Kreutz, K. J., David Meeker, L., Whitlow, S. I., & Twickler, M. S. (2002). The polar expression of ENSO and sea-ice variability as recorded in a South Pole ice core. *Annals of Glaciology*, *35*, 430–436. https://doi.org/10.3189/172756402781817149

National Climatic Data Center, NESDIS, NOAA, U.S. Department of Commerce, Meteorology Department, Florida State University, Harvard College Observatory, Harvard University, & Climate Analysis Section, Climate and Global Dynamics Division, National Center for Atmospheric Research, University Corporation for Atmospheric Research. (1981). World monthly surface station climatology. *Boulder CO: Research Data Archive at the National Center for Atmospheric Research, Computational and Information Systems Laboratory*. Retrieved from https://rda.ucar.edu/datasets/d570000/

Peltola, T., Havulinna, A. S., Salomaa, V., & Vehtari, A. (2014). Hierarchical Bayesian survival analysis and projective covariate selection in cardiovascular event risk prediction. *BMA@ UAI*, *27*, 79–88.

Piironen, J., & Vehtari, A. (2017). Sparsity information and regularization in the horseshoe and other shrinkage priors. *Electronic Journal of Statistics*, *11*(2), 5018–5051. https://doi.org/10.1214/17-EJS1337SI

Porter, S. E., Parkinson, C. L., & Mosley-Thompson, E. (2016). Bellingshausen Sea ice extent recorded in an Antarctic Peninsula ice core. *Journal of Geophysical Research*, *121*(23), 13886–13900. https://doi.org/10.1002/2016JD025626

Raphael, M. N., & Hobbs, W. (2014). The influence of the large-scale atmospheric circulation on Antarctic sea ice during ice advance and retreat seasons. *Geophysical Research Letters*, *41*(14), 5037–5045. https://doi.org/10.1002/2014GL060365

Rubin, D. B., & Little, R. J. A. (2019). *Statistical analysis with missing data*. John Wiley & Sons.

Sinclair, K. E., Bertler, N. A., Bowen, M. M., & Arrigo, K. R. (2014). Twentieth century sea-ice trends in the Ross Sea from a high-resolution, coastal ice-core record. *Geophysical Research Letters*, *41*(10), 3510–3516. https://doi.org/10.1002/2014GL059821

Stan Development Team. (2022). The Stan core library. Retrieved from http://mc-stan.org/Version2.31

Thomas, E. R., & Abram, N. J. (2016). Ice core reconstruction of sea ice change in the Amundsen-Ross Seas since 1702 A.D. *Geophysical Research Letters*, *43*(10), 5309–5317. https://doi.org/10.1002/2016GL068130

Thomas, E. R., Allen, C. S., Etourneau, J., King, A. C., Severi, M., Winton, V. H. L., et al. (2019). Antarctic sea ice proxies from marine and ice core archives suitable for reconstructing sea ice over the past 2000 years. *MDPI AG*, *9*(12), 506. https://doi.org/10.3390/geosciences9120506

West, M., & Harrison, J. (2006). *Bayesian forecasting and dynamic models*. Springer Science & Business Media.

Yang, J., Xiao, C., Liu, J., Li, S., & Qin, D. (2021). Variability of Antarctic sea ice extent over the past 200 years. *Science Bulletin*, *66*(23), 2394–2404. https://doi.org/10.1016/j.scib.2021.07.028